Volume 1
Number 6
December 2025
Pages 1341-1824

EES Batteries

rsc.li/EESBatteries

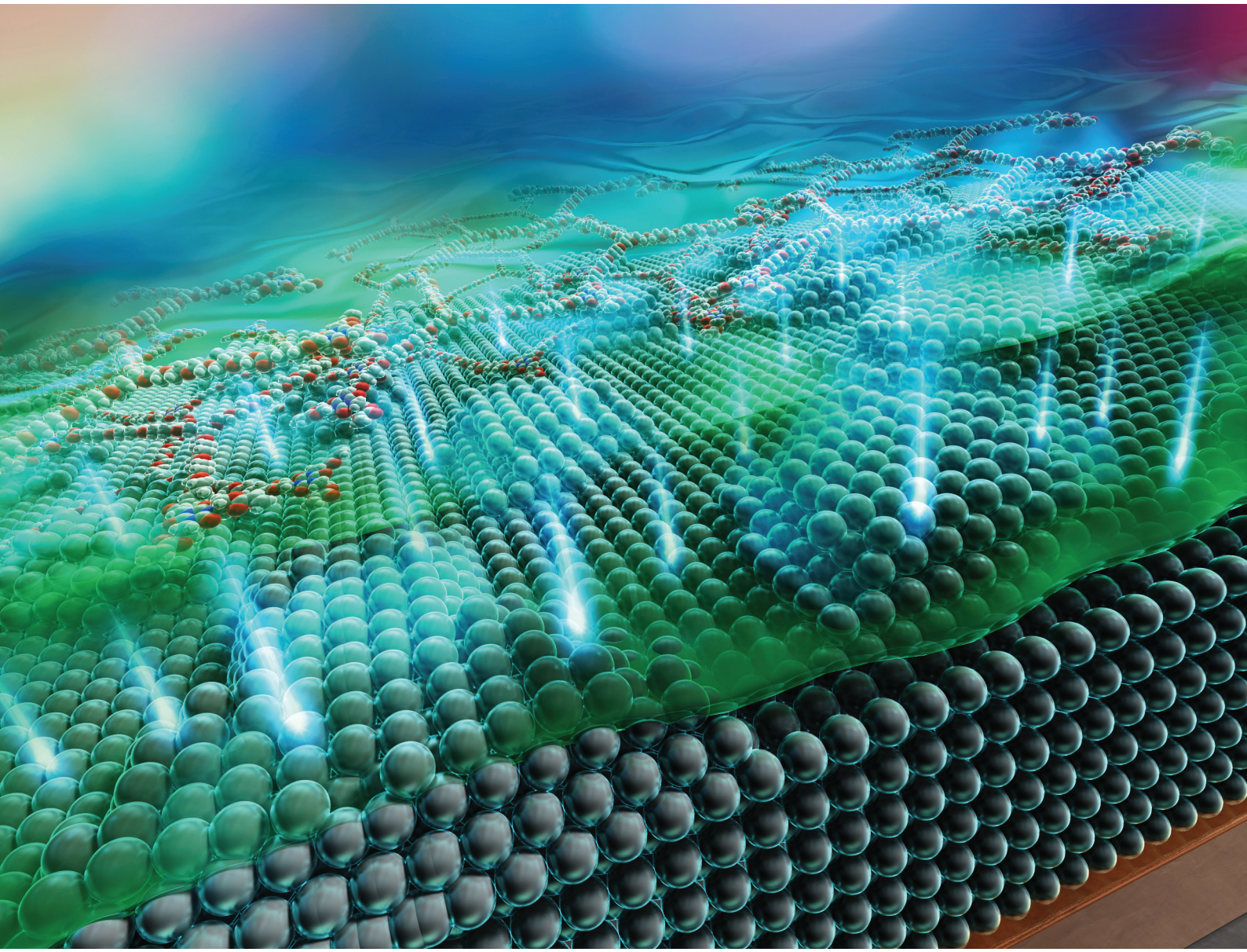

ISSN 3033-4071

ROYAL SOCIETY OF CHEMISTRY

PAPER

Hiroki Nara, Toshiyuki Momma *et al.*
Artificial solid electrolyte interphase composed of a tris(2-acryloyloxyethyl) isocyanurate-based polymer for lithium metal anode

EES Batteries

PAPER

View Article Online
View Journal | View Issue

Cite this: *EES Batteries*, 2025, **1**, 1515

Artificial solid electrolyte interphase composed of a tris(2-acryloyloxyethyl) isocyanurate-based polymer for lithium metal anode

Hiroki Nara, *[a] Takumi Miyamoto,[b] Takahiro Kosaki, [b] Hiroki Hayashi [b] and Toshiyuki Momma *[b]

Received 9th June 2025,
Accepted 25th July 2025

DOI: 10.1039/d5eb00109a

rsc.li/EESBatteries

To enhance the mechanical robustness of artificial solid electrolyte interphases (SEIs), particularly their resistance to swelling in liquid electrolytes, we developed a cross-linked polymer coating derived from tris (2-acryloyloxyethyl) isocyanurate (TAIC) and trimethylolpropane ethoxylate triacrylate (ETPTA) for lithium metal anodes. The TAIC : ETPTA (3 : 1)-based polymer exhibited excellent film-forming ability, mechanical stability, and interfacial compatibility with lithium metal. Symmetric cell tests demonstrated prolonged cycling stability exceeding 3500 hours (equivalent to 350 charge–discharge cycles), and a high lithium ion transference number (t_{Li+} = 0.75). Furthermore, the polymer film effectively suppressed dendritic lithium growth and minimized electrolyte decomposition. Electrochemical impedance spectroscopy and surface morphology analysis revealed that the coating reduced SEI thickening and interfacial resistance growth during cycling. This work presents a rational design of a mechanically and ionically optimized artificial SEI, offering a viable strategy for stabilizing lithium metal electrodes in high-energy-density batteries such as lithium–sulfur systems.

Broader context

Lithium metal is considered the ultimate anode material for next-generation batteries due to its extremely high capacity and low redox potential. However, its practical application is severely limited by dendrite formation and continuous electrolyte decomposition. Artificial solid electrolyte interphases (SEIs) offer a promising strategy to address these challenges. Inorganic SEIs provide mechanical strength but suffer from poor flexibility and interfacial defects, while organic SEIs offer flexibility but lack sufficient ionic conductivity and strength. Here, we report a novel tris(2-acryloyloxyethyl) isocyanurate (TAIC)-based polymer system that balances these requirements through a molecularly designed copolymer network with trymethylolpropane ethoxylate triacrylate (ETPTA). The resulting artificial SEI not only enables uniform lithium deposition but also significantly enhances interfacial stability and ionic transport. By effectively preventing excessive SEI growth, the coating enables extended cycling of lithium metal electrodes, which is critical for lithium–sulfur and other high-energy battery chemistries. Our findings highlight the importance of interfacial engineering using tailored polymer coatings and open new avenues for stabilizing reactive metal anodes in practical battery systems.

Introduction

The reduction of carbon dioxide (CO_2) emissions is recognized as a critical global challenge to ensure access to affordable, reliable, sustainable, and modern energy for all, and to facilitate urgent actions to mitigate climate change and its associated impacts. This aligns with the Sustainable Development Goals (SDGs) adopted by the United Nations in 2015, particularly Goals 7 (Affordable and Clean Energy) and 13 (Climate Action).[1,2] To achieve this challenge, the electrification of mobility and effective utilization of green energy, such as solar and wind power, using energy storage are essential. Energy storage is required to achieve a high energy density, high cycle durability, and cost-effectiveness. As next-generation rechargeable batteries, sulfur and air cathodes are promising from the viewpoint of high energy density and cost-effectiveness. These cathodes are combined with lithium metal anodes because of their high theoretical capacity (3860 mAh g^{-1}) and low redox potential (−3.045 V *vs.* SHE).[3,4] Thus, lithium metal has been recognized as the ultimate anode material. However, lithium metal faces the critical problem of dendritic deposition, which causes short circuits, leading to capacity loss and severe accidents such as fire and battery explosions.[3] Furthermore, the negative potential of lithium metal leads to solid electrolyte

[a]*Research Organization for Nano and Life Innovation, Waseda University, 513, Wasedatsurumakicho, Shinjuku-ku, Tokyo 162-0041, Japan. E-mail: nara.hiroki@aoni.waseda.jp*
[b]*Graduate School of Advanced Science and Engineering, Waseda University, 3-4-1 Okubo, Shinjuku-ku, Tokyo 169-8555, Japan. E-mail: momma@waseda.jp*

interphase (SEI) formation, which consists of reduced products of electrolyte components. The structure of the SEI is represented as a mosaic model in which inorganic and organic compounds are unevenly distributed.[5] Moreover, the uneven SEI structure results in unequal lithium-ion flux, leading to dendritic deposition.[6,7] The mechanism of lithium dendritic growth is reported to be lithium-ion flux concentration due to the cracking of the SEI, where the ion transport resistance is low,[8] and the strong local electric field at the tip of the dendrite.[9,10] Dendritic deposition eventually causes capacity loss due to dead lithium caused by electrical isolation during discharge[11,12] and severe accidents. These impediments hinder their practical applications in rechargeable batteries. Many researchers have attempted to suppress the dendritic deposition in several ways. One is from the viewpoint of electrolytes. Carbonate-based solvents, such as ethylene carbonate and propylene carbonate, have conventionally been utilized as electrolytes. However, the SEI formed from the carbonate-based electrolytes is brittle due to the uneven stacking of Li_2O Li_2CO_3, *etc.* known as "mosaic" model.[3] Conversely, ether-based solvents, such as DOL and DME, are stable against Li metal and forms an oligomer-like SEI which is flexible and has a high affinity for the electrode.[3,13] While highly concentrated lithium salt electrolytes have been reported to improve charge–discharge efficiency and suppress dendritic deposition. This is attributed to an SEI improvement by compact inorganic components derived from lithium salts, such as LiFSA and LiTFSA, and the rectifying effect of the lithium-ion flux.[14] Such inorganic surface modification has also been reported in the field of zinc metal anodes.[15] Additives to the electrolyte are also considered as a solution. Additives have two main functions that can be categorized into different types. One involves additives that decompose on the lithium metal electrode, resulting in a favorable SEI. Typical additives are FEC that forms LiF which indicates mechanical strength and low diffusion barrier, and $LiNO_3$ that forms compact SEI composed of nitrides and fluorides.[16,17]

The second is an additive that adsorbs onto the lithium electrode surface, resulting in uniform lithium deposition. This promotes uniform Li precipitation morphology. For example, at low concentrations, Cs^+ and Rb^+, which have a lower standard reduction potential than Li^+, adsorb onto the convex parts of the electrode, which have a strong electric field, making the convex part positively charged. The positive charge suppresses the concentration of the lithium-ion flux at the convex parts, which is called the self-healing electrostatic shield (SHES) mechanism.[18,19] However, these additives continue to decompose owing to reductive decomposition and co-precipitation with Li^+. It can be said that their effectiveness is limited because they are consumed during this process.[20] While there are approaches to protect the lithium metal surface by artificial SEI prior to the SEI formation derived from the reductive decomposition of electrolyte. An artificial SEI is required to be mechanically stable against an electrode volume change, to achieve uniform lithium-ion flux, and to stabilize the interface between the electrolyte and electrode by reducing the contact area. Artificial inorganic SEIs (*e.g.*, LiF,[21] Al_2O_3,[22] and Li_2S [23]) have been widely investigated because of their high elastic moduli (>6 GPa) and ionic conductivities. However, the cycle durability of inorganic artificial SEIs still needs to be improved because of grain boundaries and defects in the SEI, and less flexibility.[24] On the contrary, organic artificial SEIs,[25–27] like a polymer film, indicate uniformity for coating on electrodes and flexibility that is effective against volume change of electrodes, however, have issues of low ionic conductivity and low mechanical strength enough to suppress dendritic deposition. Thus, an artificial SEI that satisfies the mechanical strength, flexibility, and ionic conductivity requirements is strongly desired for the progress of lithium metal anodes.

To overcome the issues of compatibility between mechanical strength and ionic conductivity, we developed a cross-linked polymer film based on tris(2-acryloyloxyethyl) isocyanurate (TAIC), which is a monomer with one functional group and three polymerizable groups, expecting ionic conductivity and mechanical strength after polymerization, as an artificial SEI. Also, TAIC has a polar group, which is expected to homogenize the distribution of Li ion flux.[28] Aiming to application of lithium–sulfur (Li–S) battery, we investigate the TAIC-based artificial SEI in 1,3-dioxolane (DOL)/dimethoxyethane (DME) electrolyte system which is commonly used for Li–S battery.[29,30] In addition, trimethylolpropane ethoxylate triacrylate (ETPTA), which possesses three polymerizable groups and an ester group that interacts with anions of lithium salts,[28] is copolymerized to adjust the electrochemical properties of the artificial SEI.

Results and discussion

TAIC and ETPTA possess C=C bonds in their acrylate groups, which serve as sites for photopolymerization (Fig. 1a). Polymerization occurs through cleavage of the C=C bond by

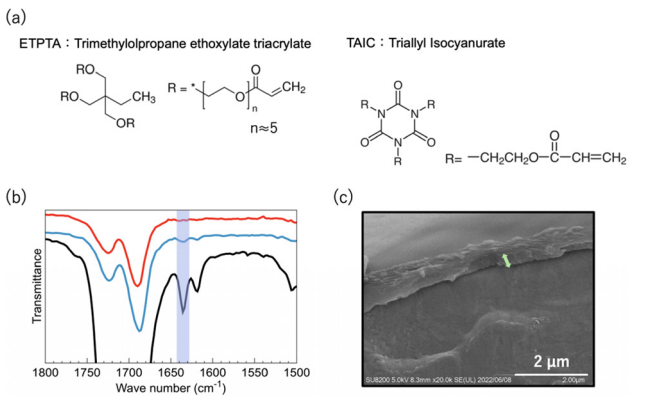

Fig. 1 (a) Chemical structure of TAIC and ETPTA. (b) FT-IR spectra of mixture of TAIC and ETPTA monomers (black line), TAIC after UV radiation (blue line), and TAIC and ETPTA (3 : 1 by weight) after UV radiation (red line). (c) Cross-sectional SEM image of the TAIC : ETPTA (3 : 1)-derived polymer coated on Cu substrate, prepared with a diluent ratio of the polymer precursor to THF (1 : 100).

photoradicals initiated by UV radiation. The C=C bond in acrylate groups has been reported to photo-polymerize efficiently due to its high electron density and close proximity to adjacent functional groups.[31] To confirm the polymerization of TAIC and ETPTA, the monomers were photopolymerized on a Cu substrate, followed by FT-IR analysis (Fig. 1b and the overview in Fig. S1). The peak at approximately 1640 cm^{-1}, which represents the C=C bond, was observed before polymerization. The peaks in TAIC and ETPTA after UV radiation completely disappeared, indicating that the monomers were fully polymerized. However, a slight peak in TAIC after UV radiation was observed, implying residual C=C. This is because the steric barrier of TAIC disturbs polymerization. In other words, ETPTA buffers the steric barrier of TAIC, achieving the complete polymerization of TAIC and ETPTA. Thickness was optimized by changing the dilution ratio of the polymer precursor and the diluent (1 : 50, 1 : 100, and 1 : 150 by mass). Complete coating on substrate was achieved with the mass ratio of 1 : 50 and 1 : 100 only (Fig. S1a and Fig. 1c). Thickness of the polymerized TAIC : ETPTA (3 : 1) film with the mass ratio of 1 : 50 and 1 : 100 was ~1 and ~0.4 μm, respectively. The mass ratio of 1 : 150 resulted in island like coating (Fig. S1b). In addition, EIS analysis revealed that the coating film polymerized with the ratio of 1 : 100 indicated lower resistance (Fig. S1c).

First of all electrochemical evaluations, the effect of the artificial SEI made of TAIC was investigated by charge–discharge test of a symmetrical cell composed of Li coated with the TAIC-derived polymer film and polyolefin-based separator impregnated with a liquid electrolyte (Fig. 2a). The cell with the TAIC-derived polymer coating initially exhibited an overvoltage of approximately 50 mV, which subsequently decreased to approximately 15 mV after five charge–discharge cycles. This behavior is attributed to the expansion of the electrode surface area caused by the formation of deposits and pits, respectively.[32] Afterwards, the cell cycles were stable for more than 2000 h; however, after 1500 h, the overvoltage increased in each charging and discharging cycle. On the other hand, the cell without the TAIC-derived polymer coating initially shows a lower overvoltage compared to that with the TAIC-derived polymer coating, followed by a gradual increase in the overvoltage (Fig. 2a). The increase in overvoltage is primarily caused by an increase in the SEI resistance and electrolyte resistance owing to continuous electrolyte consumption. Conversely, the TAIC-derived polymer coating effectively suppresses the continuous consumption of electrolyte. To confirm the effect of polymerization, a symmetrical cell of non-coated Li but TAIC monomer was added to the electrolyte. The results indicate a flat voltage profile during charging and discharging, indicating

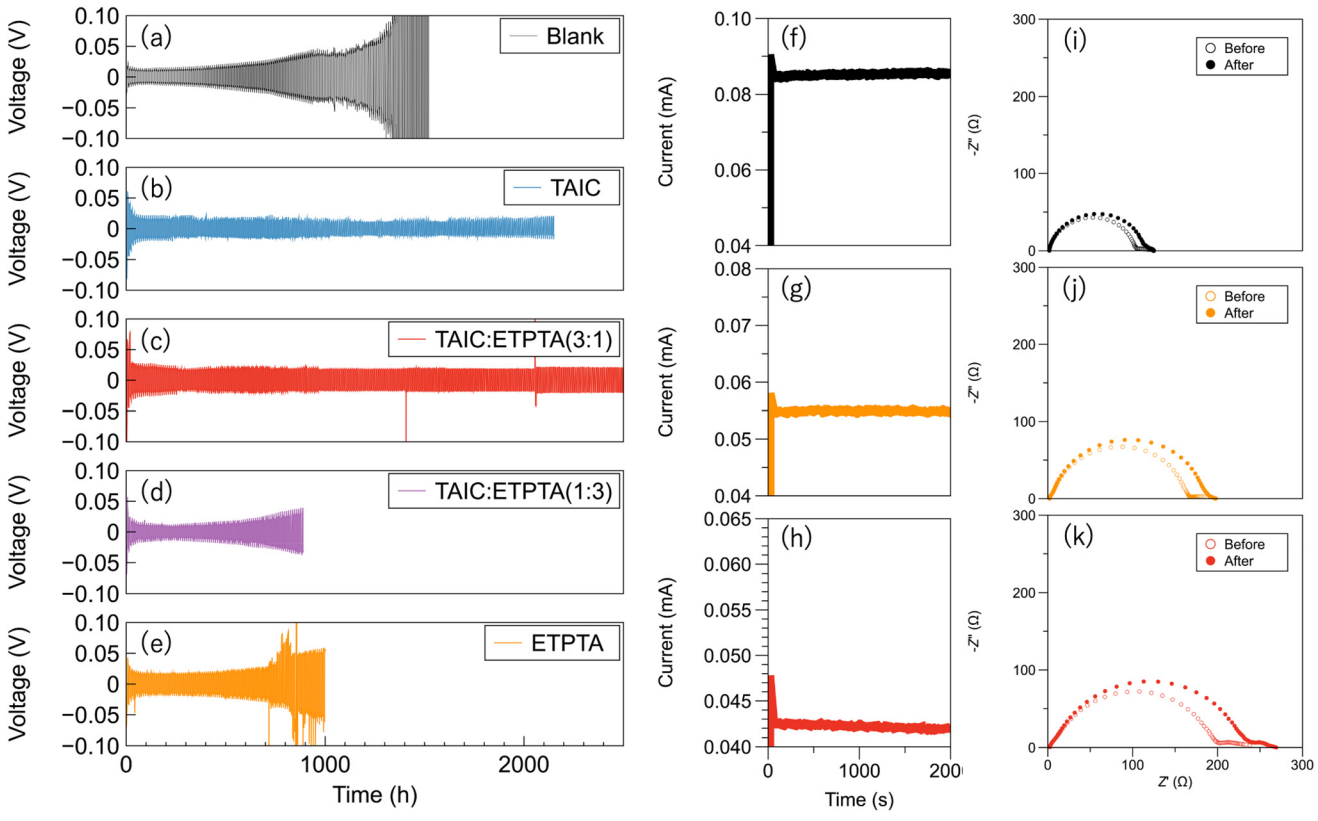

Fig. 2 Charge–discharge test, with a current density of 0.4 mA cm^{-2} for 5 hours, of a symmetrical cells composed of Li coated with (a) no polymer and (b) TAIC, (c) TAIC : ETPTA (3 : 1), (d) TAIC : ETPTA (1 : 3), (e) ETPTA and polyolefin-based separator impregnated with a liquid electrolyte; Chronoamperograms, under 10 mV polarization, of symmetrical cells of Li (f) coated with no polymer, (g) ETPTA, (h) TAIC : ETPTA (3 : 1); Nyquist plots before and after 10 mV polarization of symmetrical cells of Li (i) coated with no polymer, (j) ETPTA, (k) TAIC : ETPTA (3 : 1).

that TAIC monomer addition facilitates a micro short circuit (Fig. S2). As a result of the FT-IR analysis, the polymerization of only TAIC had residual C=C due to the steric barrier. Previous research has shown that the C=C bond is prone to degradation when in contact with lithium metal,[33] which can potentially result in the breakdown of the artificial solid electrolyte interface (SEI). Therefore, ETPTA was copolymerized with TAIC to buffer the steric barrier. TAIC-ETPTA copolymers with different weight ratios of the precursors (TAIC : ETPTA = 3 : 1 and 1 : 3) were synthesized. As illustrated in Fig. 1b, the residual C=C in the synthesized polymer was effectively eliminated. Symmetrical cells of Li coated with TAIC : ETPTA (3 : 1), TAIC : ETPTA (1 : 3), and ETPTA were cycled (Fig. 2b, c, and d, respectively). The cell with a TAIC : ETPTA (3 : 1)-derived polymer coating demonstrates an overvoltage of approximately 18 mV and maintains stable charge–discharge cycles for over 3500 hours (Fig. S3). Conversely, the cells with TAIC : ETPTA (1 : 3) and ETPTA-derived polymer coatings exhibit charge–discharge behaviour similar to that of cells without any polymer coating, as illustrated in Fig. 2a. This phenomenon is attributed to the plasticization of CH_2–CH_2–O part in ETPTA. While ETPTA contains multiple ether units that generally increase the polymer's free volume and flexibility,[34] TAIC has fewer ether groups and forms a highly crosslinked structure. In the TAIC : ETPTA (3 : 1) system, the high crosslinking density significantly restricts chain mobility and accessible free volume, thereby suppressing electrolyte-induced swelling. The plasticization degree was evaluated by a degree of swelling with the electrolyte (Fig. S4). Subsequently, an in-depth investigation is conducted on the TAIC : ETPTA (3 : 1)-derived polymer coating, which exhibited the most favourable performance among the samples. A morphological change of the lithium electrode surface during charge–discharge cycling was investigated. After 10 cycles, the uncoated lithium electrode exhibited voids, which suggest uneven lithium deposition, such as dendrite formation (Fig. 3a). In contrast, the lithium electrode coated with the TAIC : ETPTA (3 : 1)-derived polymer showed no visible voids after 10 cycles, indicating uniform lithium dissolution and deposition during the cycles (Fig. 3b). After 87 cycles, although voids were observed even on the polymer-coated lithium surface (Fig. 3d), the lithium deposits on the uncoated electrode appeared more refined than those on the coated one (Fig. 3c). The refined lithium deposits favoured SEI formation, leading to increased electrolyte consumption for the uncoated electrode. The effect of the TAIC : ETPTA (3 : 1)-derived polymer coating on the interface between the lithium metal electrode and the electrolyte after 10 charge–discharge cycles was evaluated by XPS (Fig. S5), and the surface atomic composition of the lithium metal electrode is summarized in Table 1. The increased nitrogen content on the surface indicates the presence of the TAIC-derived polymer. In addition, the S 2p spectra show that the doublet at 164.0/165.1 eV, attributed to Li_2S, observed on the surface without the polymer coating, is barely detectable on the coated surface (Fig. S5). These results suggest that SEI formation is suppressed by the polymer protection layer. Furthermore, the elevated fluorine and sulfur

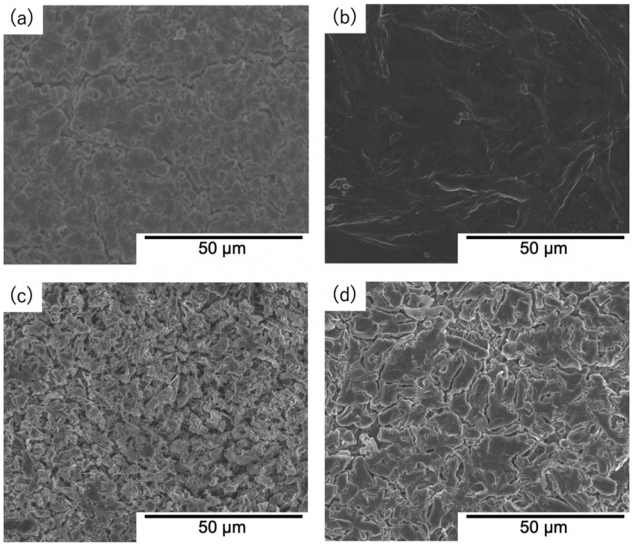

Fig. 3 SEM images of the lithium electrode surface: (a) and (b) after 10 charge–discharge cycles, and (c) and (d) after 87 cycles. (a and c) show uncoated electrodes, while (b and d) show electrodes coated with the TAIC : ETPTA (3 : 1)-derived polymer.

Table 1 Surface atomic composition (%) of Li electrodes after 10 charge–discharge cycles, with and without TAIC : ETPTA (3 : 1) polymer coating, as determined by XPS analysis

	Li	C	N	O	F	S
Blank	44.4	28.3	0.8	22.0	3.1	1.5
TAIC : ETPTA (3 : 1)	12.5	37.5	4.4	22.4	19.0	4.3

contents, as evidenced by the F 1s, S 2p, and N 1s spectra (see the note in Fig. S5), suggest the incorporation of LiTFSI into the polymer phase. The transport number of lithium ion (t_{Li^+}) in the symmetrical cell of the TAIC : ETPTA (3 : 1)-derived polymer coating was measured and compared with those without polymer coating, with the ETPTA by means of chronoamperometry and EIS[35] (Fig. 2f–k and Table S1). Polymer coating improved the t_{Li^+} from 0.38 ± 0.08 (without polymer coating) to 0.59 ± 0.05 and 0.75 ± 0.07 with ETPTA and TAIC : ETPTA (3 : 1)-derived polymer coating, respectively. This result is supported by a previous report that C=O strongly adsorbed TSFI anion through electrostatic interaction.[28] Thus the polymer phase effectively suppressed the anion migration. Furthermore, the bridging ETPTA with TAIC limit the swelling of the CH_2–CH_2–O part, resulting in higher t_{Li^+} value in the TAIC : ETPTA (3 : 1)-derived polymer coating.

In addition, the electrochemical stability of the coating of the TAIC : ETPTA (3 : 1)-derived polymer was investigated by LSV on Cu working electrode with comparison of those without the coating, with TAIC, and with ETPTA derived polymer coating (Fig. 4a). The reduction peak at 1.0 V was observed in all samples and is attributed to the reductive decomposition of DOL.[36] The reduction peak at 0.55 V was observed only in the ETPTA-derived polymer coating, being

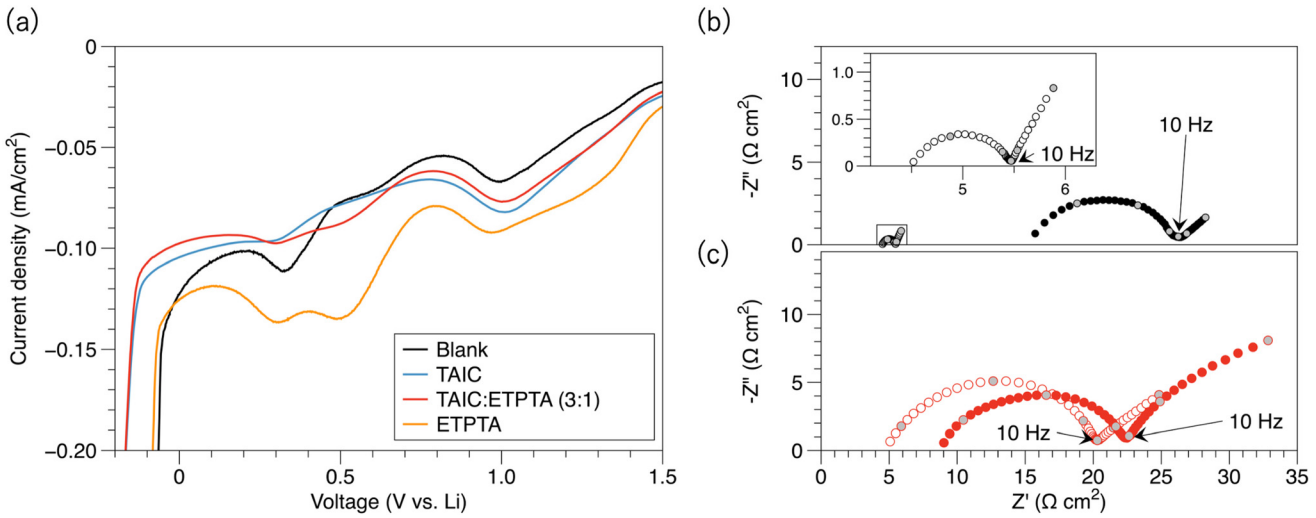

Fig. 4 (a) LSV curves of Cu electrodes with polymer coatings derived from TAIC, TAIC : ETPTA (3 : 1), and ETPTA, along with an uncoated Cu electrode. (b and c) Nyquist plots of symmetric Li–Li cells: (b) without and (c) with a TAIC : ETPTA (3 : 1)-derived polymer coating. Open and closed markers indicate the impedance after 16 and 50 charge–discharge cycles, respectively. The inset in (b) shows an enlarged view of the plots after 16 cycles. Grey markers indicate data points corresponding to one frequency decade.

assigned to the reduction of ETPTA. Although a slight shoulder of the reduction current was detected in the TAIC : ETPTA (3 : 1)-derived polymer coating, it was significantly suppressed due to copolymerization with TAIC. An obvious reduction peak at 0.3 V was observed in both without the coating and ETPTA-derived polymer coating, which can be attributed to the reductive decomposition of the TFSI anion.[36] These results suggest that the dense polymer network coatings derived from TAIC or TAIC : ETPTA (3 : 1) trap TFSI anions, thereby reducing their concentration at the electrode surface and suppressing their reductive decomposition. The trapping of TFSI anion is also supported by the transport number. Furthermore, the cycle durability of the lithium electrode coated with or without the TAIC : ETPTA (3 : 1)-derived polymer was investigated. As shown in Fig. 2(a) and (b), the overvoltage increase of the symmetrical cells of Li during the charge–discharge cycles was effectively suppressed by applying the coating. To investigate the cause of the overvoltage increase, electrochemical impedance spectroscopy (EIS) was performed on symmetric cells composed of lithium metal electrodes with or without the TAIC : ETPTA (3 : 1)-derived polymer coating after 16 and 50 charge–discharge cycles (Fig. 4b and c). In the early stages of cycling, the resistance (R_s), corresponding to the x-axis intercept in the high-frequency region, remained nearly identical between the cells with and without the polymer coating, as it reflects the bulk electrolyte resistance. In contrast, the interfacial ionic resistance (R_i), associated with the SEI and polymer coating, was significantly lower in the uncoated cell (2 Ω cm^2) than in the cell coated with the TAIC : ETPTA (3 : 1)-derived polymer (15 Ω cm^2). This pronounced difference is attributed to the contribution of the polymer layer to the overall ionic resistance. After 50 cycles, both R_s and R_i increased markedly in the uncoated cell, whereas these increases were suppressed in the coated cell. These results demonstrate that the TAIC : ETPTA (3 : 1)-derived polymer coating effectively protects the lithium metal surface by suppressing further SEI formation and electrolyte decomposition, thereby preventing increases in both interfacial and bulk resistances.

Conclusions

In this study, we developed an artificial solid electrolyte interphase (SEI) using a cross-linked polymer derived from tris(2-acryloyloxyethyl) isocyanurate (TAIC) and trimethylolpropane ethoxylate triacrylate (ETPTA), with the aim of enhancing mechanical robustness—particularly resistance to swelling—at the interface of lithium metal anodes. The copolymerization of TAIC and ETPTA (3 : 1 by weight) yielded a robust and flexible polymer coating that demonstrated superior electrochemical performance. This artificial SEI enabled uniform lithium deposition, suppressed dendritic growth, and significantly extended cycle stability over 3500 hours in symmetric cells. The polymer-coated lithium electrodes exhibited a high lithium ion transference number (t_{Li^+} = 0.75), effective suppression of electrolyte decomposition, and enhanced resistance against SEI thickening during long-term cycling. Furthermore, electrochemical analyses revealed that the TAIC : ETPTA (3 : 1)-derived film effectively trapped TFSI anions, minimized interfacial side reactions, and contributed to suppression of electrolyte and SEI resistance increase over prolonged operation. These results demonstrate that TAIC-based copolymer coatings are a promising strategy for constructing stable, high-performance artificial SEIs suitable for next-generation lithium metal batteries, particularly under high-energy-density conditions such as lithium–sulfur systems.

Experimental

A polymer precursor was prepared by mixing 0.20 g of monomers (typically, 0.05 g of ETPTA (M_n = ~428) and 0.15 g of TAIC), and 0.01 g of 2-hydroxy-2-methylpropiophenone (HMPP) as a photopolymerization initiator in 20 g of THF as a diluent (the polymer precursor and diluent ratio is 1 : 100) for 1 hour. Subsequently, 5 μL of the polymer precursor was cast directly onto a lithium electrode with a diameter of 14 mm and allowed to dry at room temperature (R.T.) for 30 min. Subsequently, the precursor was polymerized using ultraviolet radiation (UV wavelength: 365 nm; UV intensity: 743 μW cm^{-2} at a distance of 50 mm) for 40 min, resulting in a polymer-coated lithium electrode. The entire process was conducted in a dry room with a dew point below −40 °C.

Electrochemical testing was conducted using a 2032 coin-type cell. The symmetric coin-type cell consisted of two polymer-coated lithium electrodes and a separator (UPORE®, Ube Maxell Co., Ltd) with a diameter of 17 mm and thickness of 25 μm soaked with 50 μL of 1 M LiTFSI in DOL/DME (1/1 vol.). Charge–discharge cycle durability was evaluated by a constant current charge–discharge test with a current density of 0.4 mA cm^{-2} for 5 hours. Li^+ transfer number was investigated by Bruce–Vincent method:[35] after assembling the symmetric coin-type cell, electrochemical impedance spectroscopy (EIS) was conducted with an amplitude of 10 mV and a frequency range from 1 MHz to 1 mHz at open circuit voltage. Subsequently, the symmetric coin-type cell was polarized with a 10 mV bias until stabilization of the current flow, followed by EIS under polarization. The electrochemical stability of the polymer coating was evaluated by linear sweep voltammetry of a cell composed of Cu working and Li counter electrode.

The thickness of the polymer coating was verified through cross-sectional scanning electron microscopy (SEM, SU8200, Hitachi High-Tech Corporation). The occurrence of polymerization was confirmed *via* Fourier-transform infrared spectroscopy (FT-IR, Prestige-21, Shimadzu Corp.). The chemical composition of the electrode surface was analyzed using X-ray photoelectron spectroscopy (XPS, PHI-VersaProbeII, ULVAC-PHI).

Author contributions

The manuscript was written through the contributions of all authors. All authors have approved the final version of the manuscript. H. Nara: conceptualization, writing – original draft, visualization, supervision. T. Miyamoto: investigation, data curation. T. Kosaki: formal analysis. H. Hayashi: formal analysis, writing – review & editing. T. Momma: conceptualization, supervision, funding acquisition.

Conflicts of interest

There are no conflicts to declare.

Data availability

The raw data supporting the findings of this study are available in the SI of this article as a ZIP archive: original experimental data such as electrochemical measurements and XPS spectra used in the main figures and SI. No custom code was used in this study. See DOI: https://doi.org/10.1039/d5eb00109a

Acknowledgements

This study was supported by the JST ALCA-SPRING (grant no. JPMJAL1301), Japan. This work was partially supported by the Advanced Research Infrastructure for Materials and Nanotechnology of Japan (ARIM) (grant no. JPMXP1223), Japan.

References

1 United Nations, *Transforming our world: the 2030 Agenda for Sustainable Development (A/RES/70/1)*, 2015.
2 W. L. Filho, T. Wall, A. L. Salvia, M. A. P. Dinis and M. Mifsud, *Sci. Rep.*, 2023, **13**, 1–7.
3 D. Lin, Y. Liu and Y. Cui, *Nat. Nanotechnol.*, 2017, **12**(3), 194–206.
4 P. G. Bruce, S. A. Freunberger, L. J. Hardwick and J.-M. Tarascon, *Nat. Mater.*, 2012, **11**, 19–29.
5 E. Peled, D. Golodnitsky and G. Ardel, *J. Electrochem. Soc.*, 1997, **144**, L208–L210.
6 Z. Zhuang, B. Ju, P. Ma, L. Yang and F. Tu, *Ionics*, 2021, **27**, 1069–1079.
7 B. Ghanbarzadeh, A. Khatibi, A. Asadi and B. Shokri, *J. Energy Storage*, 2022, **47**, 103668.
8 G. Bieker, M. Winter and P. Bieker, *Phys. Chem. Chem. Phys.*, 2015, **17**, 8670–8679.
9 S. Li, M. Jiang, Y. Xie, H. Xu, J. Jia and J. Li, *Adv. Mater.*, 2018, **30**, 1706375.
10 P. Bai, J. Li, F. R. Brushett and M. Z. Bazant, *Energy Environ. Sci.*, 2016, **9**, 3221–3229.
11 X. R. Chen, C. Yan, J. F. Ding, H. J. Peng and Q. Zhang, *J. Energy Chem.*, 2021, **62**, 289–294.
12 A. Kushima, K. P. So, C. Su, P. Bai, N. Kuriyama, T. Maebashi, Y. Fujiwara, M. Z. Bazant and J. Li, *Nano Energy*, 2017, **32**, 271–279.
13 L. E. Camacho-Forero and P. B. Balbuena, *Phys. Chem. Chem. Phys.*, 2017, **19**, 30861–30873.
14 L. Suo, Y. S. Hu, H. Li, M. Armand and L. Chen, *Nat. Commun.*, 2013, **4**(1), 1–9.
15 R. Li, Y.-H. Lee, E. Park, Y. Jeoun, S.-H. Huh, K.-S. Ahn, Y.-E. Sung and S.-H. Yu, *EES Batteries*, 2025, **1**, 195–207.
16 N. Piao, S. Liu, B. Zhang, X. Ji, X. Fan, L. Wang, P. F. Wang, T. Jin, S. C. Liou, H. Yang, J. Jiang, K. Xu, M. A. Schroeder, X. He and C. Wang, *ACS Energy Lett.*, 2021, **6**, 1839–1848.

17 J. Fu, X. Ji, J. Chen, L. Chen, X. Fan, D. Mu and C. Wang, *Angew. Chem., Int. Ed.*, 2020, **59**, 22194–22201.
18 F. Ding, W. Xu, G. L. Graff, J. Zhang, M. L. Sushko, X. Chen, Y. Shao, M. H. Engelhard, Z. Nie, J. Xiao, X. Liu, P. V. Sushko, J. Liu and J. G. Zhang, *J. Am. Chem. Soc.*, 2013, **135**, 4450–4456.
19 Y. Zhang, J. Qian, W. Xu, S. M. Russell, X. Chen, E. Nasybulin, P. Bhattacharya, M. H. Engelhard, D. Mei, R. Cao, F. Ding, A. V. Cresce, K. Xu and J. G. Zhang, *Nano Lett.*, 2014, **14**, 6889–6896.
20 Z. Huang, S. Choudhury, H. Gong, Y. Cui and Z. Bao, *J. Am. Chem. Soc.*, 2020, **142**, 21393–21403.
21 L. Chen, K. S. Chen, X. Chen, G. Ramirez, Z. Huang, N. R. Geise, H. G. Steinrück, B. L. Fisher, R. Shahbazian-Yassar, M. F. Toney, M. C. Hersam and J. W. Elam, *ACS Appl. Mater. Interfaces*, 2018, **10**, 26972–26981.
22 A. C. Kozen, C. F. Lin, A. J. Pearse, M. A. Schroeder, X. Han, L. Hu, S. B. Lee, G. W. Rubloff and M. Noked, *ACS Nano*, 2015, **9**, 5884–5892.
23 H. Chen, A. Pei, D. Lin, J. Xie, A. Yang, J. Xu, K. Lin, J. Wang, H. Wang, F. Shi, D. Boyle and Y. Cui, *Adv. Energy Mater.*, 2019, **9**, 1900858.
24 Z. Yu, Y. Cui and Z. Bao, *Cell Rep. Phys. Sci.*, 2020, **1**, 100119.
25 N. W. Li, Y. Shi, Y. X. Yin, X. X. Zeng, J. Y. Li, C. J. Li, L. J. Wan, R. Wen and Y. G. Guo, *Angew. Chem., Int. Ed.*, 2018, **57**, 1505–1509.
26 Z. Wang, Y. Wang, Z. Zhang, X. Chen, W. Lie, Y.-B. He, Z. Zhou, G. Xia and Z. Guo, *Adv. Funct. Mater.*, 2020, **30**, 2002414.
27 Y. Zhong, P. Huang, W. Yan, Z. Su, C. Sun, Y. Xing and C. Lai, *Adv. Funct. Mater.*, 2022, **32**, 2110347.
28 M. Chen, J. Zheng, Y. Liu, O. Sheng, Z. Ju, G. Lu, T. Liu, Y. Wang, J. Nai, Q. Wang and X. Tao, *Adv. Funct. Mater.*, 2021, **31**, 2102228.
29 S. C. Kim, X. Gao, S. L. Liao, H. Su, Y. Chen, W. Zhang, L. C. Greenburg, J. A. Pan, X. Zheng, Y. Ye, M. S. Kim, P. Sayavong, A. Brest, J. Qin, Z. Bao and Y. Cui, *Nat. Commun.*, 2024, **15**(1), 1–9.
30 A. Manthiram, S. H. Chung and C. Zu, *Adv. Mater.*, 2015, **27**, 1980–2006.
31 E. S. Jönsson, T. Y. Lee, K. Viswanathan, C. E. Hoyle, T. M. Roper, C. A. Guymon, C. Nason and I. V. Khudyakov, *Prog. Org. Coat.*, 2005, **52**, 63–72.
32 J. H. Hyun, M. J. Yi, H. Jung, S. H. Lee, J. H. Um and S. H. Yu, *Energy Storage Mater.*, 2023, **54**, 146–155.
33 J. P. Vivek and N. Garcia-Araez, *J. Phys. Chem. C*, 2024, **128**, 13395–13401.
34 G. Foran, D. Mankovsky, N. Verdier, D. Lepage, A. Prébé, D. Aymé-Perrot and M. Dollé, *iScience*, 2020, **23**, 101597.
35 J. Evans, C. A. Vincent and P. G. Bruce, *Polymer*, 1987, **28**, 2324–2328.
36 Y. Gu, W. W. Wang, J. W. He, S. Tang, H. Y. Xu, J. W. Yan, Q. H. Wu, X. B. Lian, M. S. Zheng, Q. F. Dong and B. W. Mao, *ChemElectroChem*, 2019, **6**, 181–188.